UKF-based Wind Estimation and Sub-optimal Turbine Control under Waked Conditions

Silva, Jean Gonzalez; Liu, Yichao; Ferrari, Riccardo; van Wingerden, Jan Willem

DOI
10.1016/j.ifacol.2023.10.1166

Publication date
2023

Document Version
Final published version

Published in
IFAC-PapersOnLine

Available online at www.sciencedirect.com

ScienceDirect

IFAC Papers Online CONFERENCE PAPER ARCHIVE

IFAC PapersOnLine 56-2 (2023) 7662–7667

UKF-based Wind Estimation and Sub-optimal Turbine Control under Waked Conditions ⋆

Jean Gonzalez Silva * **Yichao Liu** * **Riccardo Ferrari** *
Jan-Willem van Wingerden *

* *Delft University of Technology, Delft, The Netherlands (e-mail: {J.GonzalezSilva, Y.Liu-17, R.Ferrari, J.W.vanWingerden}@tudelft.nl)*

Abstract: The knowledge of the Effective wind speed (EWS) allows the designing of wind turbine controllers that regulate power production and reduce loads on turbine components. Traditional single-point measurements are known to suffer from high noise and poor correlation with the EWS. As an alternative to overcome these problems, EWS estimators can be designed. The main challenge is the high non-linearity of the wind speed influence on the drive-train dynamics. Therefore, an estimator based on the unscented Kalman filter (UKF) is proposed and compared against an extended Kalman filter (EKF) and the immersion and invariance (I&I) technique. Simulation results are provided and show the superior performances attained by the UKF. Furthermore, the usefulness of the estimated EWS is demonstrated by designing a sliding mode controller (SMC) that can track a desired power reference. In addition, the controller allows operating in sub-optimal conditions, where load reduction is attained at the expense of power maximization. The proposed estimator's and controller's performances are evaluated under wind farm wake conditions via high-fidelity simulations. The findings show that UKF can outperform the EKF and the controller can reduce loads, except under highly waked conditions.

Keywords: Nonlinear observers and filter design; Wind turbine control; Sliding mode control;

1. INTRODUCTION

The Kalman filter (KF) has been widely used to provide unbiased state estimations for linear systems using a dynamic model and measurements from the system [9]. However, in many applications, the corresponding system presents highly nonlinear behavior, as in the case of the aerodynamics of a wind turbine [1]. The extended Kalman filter (EKF) might be the most widely used estimation algorithm for nonlinear systems. Although effective, it shows some limitations, e.g. difficult implementation and tuning, and reliability only for systems that are almost linear on the time scale of the updates, i.e."quasilinear" problems. Many of these difficulties arise from the use of linearization. To overcome some of the EKF limitations, the unscented transformation (UT) was developed to propagate the mean and covariance information. Using a deterministic sampling approach, a minimal set of carefully chosen sample points of the previous estimate are propagated to obtain approximations of the predicted and corrected states. The unscented Kalman filter (UKF) can be more accurate, is easier to implement - derivative-free, and its computational complexity is in the same order as the EKF [8, 25]. Since its introduction, several implementations of the UKF have been proposed [14].

In a wind turbine, the anemometer on top of the nacelle is usually used to measure the wind speed, called point-wise wind speed. Such wind speed information does not fully represent the effective wind speed (EWS) since it is impossible to represent the spatially three-dimensional wind field on the swept rotor area by a unique measure. Lately, LIDAR emerged as a promising technology to measure the full wind speed profile [22]. However, in some scenarios, e.g. upstream turbines, disturbances driven by blade shadows and spatially varying turbulent effects can still significantly affect the measurements, besides the high cost of this technology.

In order to estimate the EWS, a large number of approaches have been developed in the literature. In [24], the authors compare different well-established estimators including the immersion and invariance (I&I) estimator [15] and the EKF-based estimator [10]. In recent work, an improvement of the I&I estimator is proposed in [12], where the authors add an integrator to the correction term enhancing its accuracy and stability. In the before-mentioned EKF-based estimator, the tower fore-aft dynamics, besides the drive-train dynamics, as well as wind turbulence, are modeled which may increase the estimator's accuracy. In [11], another EKF-based estimator using the drive-train model is presented, where variations of the power coefficient may lead to low performance or even divergence of the filter. Recently, an adaptive estimator based on the cubature Kalman filter - a version of the UKF - is proposed in a hierarchical structure [18], which explores, besides the superior performance, the robustness against filter divergence through adaptive covariance ma-

⋆ The authors would like to acknowledge the WATEREYE project for financial support.

10.1016/j.ifacol.2023.10.1166

trices. Apart from this recent work, the UKF technique for the problem of wind speed estimation has been not investigated in depth to the best of the author's knowledge, even though it presents a great potential for performance improvement.

The knowledge of the EWS is of relevant importance for advanced wind turbine (or farm) control design. Essentially, it determines the current operating point of the wind turbine plant, which is required for gain-scheduling control [23], feed-forward control [16], maximum power tracking and optimal control [17]. In wind farms, for example, the thrust force information as a general assessment of the loads can be considered in the wind farm control [2, 21], in which it can be estimated using the EWS estimations. Moreover, a basic solution for guaranteeing power generation and structure safety is to operate the wind turbine at a sub-optimal operating point [5, 20]. Even though power generation decreases in such cases, loads can be significantly reduced allowing the turbines to maintain high safety levels and extend their lifetime.

This paper presents the application of the UKF in wind turbines for EWS estimation. The UKF is compared to the EKF-based, I&I, and improved I&I estimators in a high-fidelity simulation environment. High-waked scenarios of a two-turbine wind farm and structural (elastic) dynamic models are used for validation. In addition, the estimated EWS is leveraged to design a sliding mode controller (SMC) that achieves a desired load reduction in sub-optimal operation conditions.

The remainder of this paper is organized as follows. First, the simplified turbine model and its general formulation are presented in Section 2. Then, the description of the UKF and the SMC are provided in Section 3 and Section 4, respectively. After that, Section 5 shows the performance of the proposed estimator and sub-optimal controller in several scenarios. The paper is concluded in Section 6.

2. MATHEMATICAL MODEL

A simplified model of the wind turbine is used by considering only the mechanical dynamics and neglecting the electrical ones, assuming they are quite faster in comparison. Hence, the dominant dynamics of the system can be obtained by applying Newton's second law to the drive-train components. Neglecting friction and higher-order terms it can be written as

$$J_{\mathrm{T}}\dot{\omega}_{\mathrm{r}} = T_{\mathrm{a}} - \eta_{\mathrm{g}} T_{\mathrm{e}}, \tag{1}$$

where T_{a} and $T_{\mathrm{e}} \geq 0$ are respectively the aerodynamic and generator torque, J_{T} is the inertia of the combined rotating parts, η_{g} is the gear-box ratio, and ω_{r} is the angular velocity of the blades. An expression for the aerodynamic torque [17, 1] parametrized by the air density ρ and the rotor radius R can be obtained by exploiting the momentum theory as

$$T_{\mathrm{a}} = 0.5\rho\pi R^2 \frac{v_{\mathrm{w}}^3}{\omega_{\mathrm{r}}} C_{\mathrm{P}}\left(\frac{R\omega_{\mathrm{r}}}{v_{\mathrm{w}}}, \theta\right), \tag{2}$$

where C_{P} represents the wind turbine power conversion efficiency. It is a function of the wind speed v_{w}, the angular velocity of the blades ω_{r}, and the collective blade pitch angle θ in a pitch-controlled wind turbine. The following assumption - verified in practice - is used to formulate the proposed estimator.

Assumption 1. The measurements of the generator torque, the collective blade-pitch angle, and the angular velocity of the rotor are available.

Moving from continuous-time to discrete-time domain, the first-order Taylor series is considered as

$$\omega_{\mathrm{r},k+1} = \omega_{\mathrm{r},k} + \dot{\omega}_{\mathrm{r},k}\Delta t + w_{\mathrm{p},k}, \tag{3}$$

where k and Δt are respectively the discrete time index and the sampling time. Also, the process noise w_{p} is added, moving from the deterministic to a stochastic framework.

To implement the unknown input estimator, a random walk model is considered to represent the wind speed development in time, as the following.

$$v_{\mathrm{w},k+1} = v_{\mathrm{w},k} + w_{\mathrm{v},k}, \tag{4}$$

where w_{v} is considered as a process noise. Replacing (1) and (2) into (3), we augment the obtained model with (4) by considering the wind speed as a dynamic state of the system. Then, the augmented state space formulation can be written as

$$\begin{bmatrix}\omega_{\mathrm{r},k+1}\\ v_{\mathrm{w},k+1}\end{bmatrix} = \begin{bmatrix}\omega_{\mathrm{r},k} + \frac{\Delta t}{J_{\mathrm{T}}} 0.5\rho\pi R^2 \frac{v_{\mathrm{w},k}^3}{\omega_{\mathrm{r},k}} C_{\mathrm{P}}\left(\frac{R\omega_{\mathrm{r},k}}{v_{\mathrm{w},k}}, \theta_k\right) - \frac{\Delta t}{J_{\mathrm{T}}}\eta_{\mathrm{g}} T_{\mathrm{e},k}\\ v_{\mathrm{w},k}\end{bmatrix} + \begin{bmatrix}w_{\mathrm{p},k}\\ w_{\mathrm{v},k}\end{bmatrix}. \tag{5}$$

As the angular velocity of the rotor is directly measured, we have the following linear measurement process.

$$\omega_{\mathrm{m},k} = \begin{bmatrix}1 & 0\end{bmatrix}\begin{bmatrix}\omega_{\mathrm{r},k}\\ v_{\mathrm{w},k}\end{bmatrix} + v_k, \tag{6}$$

where v_k is a random variable representing the measurement noise. The general nonlinear formulation with process and measurement noise is obtained as

$$\boldsymbol{x}_{k+1} = f(\boldsymbol{x}_k, \boldsymbol{u}_k) + \boldsymbol{w}_k, \tag{7}$$

$$\boldsymbol{z}_k = h(\boldsymbol{x}_k, \boldsymbol{u}_k) + \boldsymbol{v}_k, \tag{8}$$

where, in particular, $\boldsymbol{x}_k = [\omega_{\mathrm{r},k}\ v_{\mathrm{w},k}]^T$, $\boldsymbol{u}_k = [T_{\mathrm{e},k}\ \theta_k]^T$, $\boldsymbol{w}_k = [w_{\mathrm{p},k}\ w_{\mathrm{v},k}]^T$, $\boldsymbol{z}_k = [\omega_{\mathrm{m},k}]$, and $\boldsymbol{v}_k = [v_k]$.

Assumption 2. $w_{\mathrm{p},k}$, $w_{\mathrm{v},k}$ and v_k are uncorrelated zero-mean white noise signals.

Then, the noise covariance matrix is diagonal:

$$\boldsymbol{Q}_k = cov(\boldsymbol{w}_k) \approx \begin{bmatrix}\sigma^2(w_{\mathrm{p}})\Delta t & 0\\ 0 & \sigma^2(w_{\mathrm{v}})\Delta t\end{bmatrix}, \tag{9}$$

$$\boldsymbol{R}_k = cov(\boldsymbol{v}_k) \approx \sigma^2(v)\Delta t; \tag{10}$$

where $\sigma^2(a) = \mathrm{E}\left[(a-\mu_a)\right]\left[(a-\mu_a)\right]^T$ is the second central moment of the vector signal a, with $\mu_a = \mathrm{E}[a]$ being the expectation value of a. The $\sigma^2(w_{\mathrm{v}}) > 0$ herein is a scaling parameter to be chosen, which determines the spread of the random walk model.

3. UNSCENTED KALMAN FILTER

The UKF is based on the Unscented Transformation (UT), which approximates the mean $\hat{\boldsymbol{z}}_k \in \mathbb{R}^m$ and the covariance $\boldsymbol{P}_k^{zz} = \mathrm{E}\langle[\boldsymbol{z}_k - \hat{\boldsymbol{z}}_{k(+)}][\boldsymbol{z}_k - \hat{\boldsymbol{z}}_{k(+)}]^T\rangle \in \mathbb{R}^{m\times m}$ of a random

vector $\boldsymbol{z}_k \in \mathbb{R}^m$ obtained by $\boldsymbol{z}_k = h(\boldsymbol{x}_k, \boldsymbol{u}_k)$. The state $\boldsymbol{x}_k \in \mathbb{R}^n$ has mean $\hat{\boldsymbol{x}}_k \in \mathbb{R}^n$ and covariance $\boldsymbol{P}_k^{xx} = E\langle[\boldsymbol{x}_k - \hat{\boldsymbol{x}}_{k(+)}][\boldsymbol{x}_k - \hat{\boldsymbol{x}}_{k(+)}]^T\rangle \in \mathbb{R}^{n\times n}$ known by hypothesis. In this way, a set of deterministic vectors $\boldsymbol{\chi}_{j,\,k} \in \mathbb{R}^n$ with $j = 0, \ldots, 2n$, called sigma points, is introduced. Then,

$$\sum_{j=0}^{2n} \gamma_j^{(m)} \boldsymbol{\chi}_{j,\,k} = \hat{\boldsymbol{x}}_k \text{ and } \sum_{j=0}^{2n} \gamma_j^{(c)} [\boldsymbol{\chi}_{j,\,k} - \hat{\boldsymbol{x}}_k][\boldsymbol{\chi}_{j,\,k} - \hat{\boldsymbol{x}}_k]^T = \boldsymbol{P}_k^{xx}, \tag{11}$$

where $\boldsymbol{\gamma}^{(m)}$ and $\boldsymbol{\gamma}^{(c)} \in \mathbb{R}^{2n+1}$ are the weight vectors. Its elements can be chosen as proposed in [25],

$$\gamma_0^{(m)} \triangleq \frac{\lambda}{n+\lambda}, \quad \gamma_0^{(c)} \triangleq \frac{\lambda}{n+\lambda} + (1 - \alpha^2 + \beta),$$

$$\gamma_j^{(m)} \triangleq \gamma_j^{(c)} \triangleq \frac{1}{2(n+\lambda)}, \; j = 1, \ldots 2n, \tag{12}$$

where $\lambda = \alpha^2(n + \kappa) - n$ is a scaling parameter. α determines the spread of the sigma points around $\hat{\boldsymbol{x}}_k$, κ is a secondary scaling parameter, and β is used to incorporate prior knowledge of the distribution of $\boldsymbol{x}_k$. A matrix of sigma points $\boldsymbol{\chi}_k \triangleq \left[\boldsymbol{\chi}_{0,\,k}, \; \boldsymbol{\chi}_{1,\,k} \cdots \boldsymbol{\chi}_{2n,\,k}\right] \in \mathbb{R}^{n\times(2n+1)}$ is chosen as

$$\boldsymbol{\chi}_k = \hat{\boldsymbol{x}}_k \, 1_{1\times(2n+1)} + \sqrt{n+\lambda}\left[0_{n\times 1} \;\; (\boldsymbol{P}_k^{xx})^{1/2} \;\; -(\boldsymbol{P}_k^{xx})^{1/2}\right]. \tag{13}$$

The following notation is defined for simplification.

$$[\boldsymbol{\gamma}^{(m)}, \boldsymbol{\gamma}^{(c)}, \boldsymbol{\chi}_k] = \Psi_{UT}(\hat{\boldsymbol{x}}_k, \boldsymbol{P}_k^{xx}, \alpha, \kappa, \beta). \tag{14}$$

Instead of the propagation of the first and second statistic moments through a linearised model, as in the EKF, the sigma points are propagated through a nonlinear function $\boldsymbol{Z}_{j,k} = h(\boldsymbol{\chi}_{j,k}, \boldsymbol{u}_k)$ for $j = 0, \ldots 2n$, where

$$\sum_{j=0}^{2n} \gamma_j^{(m)} \boldsymbol{Z}_{j,\,k} = \hat{\boldsymbol{z}}_k \quad \text{e} \quad \sum_{j=0}^{2n} \gamma_j^{(c)} [\boldsymbol{Z}_{j,\,k} - \hat{\boldsymbol{z}}_k][\boldsymbol{Z}_{j,\,k} - \hat{\boldsymbol{z}}_k]^T = \boldsymbol{P}_k^{zz}.$$

Therefore, the KF equations are given by

$$[\boldsymbol{\gamma}^{(m)}, \boldsymbol{\gamma}^{(c)}, \boldsymbol{\chi}_{k(+)}] = \Psi_{UT}(\hat{\boldsymbol{x}}_k, \boldsymbol{P}_{k-1(+)}^{xx}, \alpha, \kappa, \beta), \tag{15}$$

$$\boldsymbol{\chi}_{j,k(-)} = f(\boldsymbol{\chi}_{j,k-1(+)}, \boldsymbol{u}_{k-1}), \text{ for } j = 0, \ldots, 2n, \tag{16}$$

$$\hat{\boldsymbol{x}}_{k(-)} = \sum_{j=0}^{2n} \gamma_j^{(m)} \boldsymbol{\chi}_{j,\,k(-)}, \tag{17}$$

$$\boldsymbol{P}_{k(-)}^{xx} = \sum_{j=0}^{2n} \gamma_j^{(c)} [\boldsymbol{\chi}_{j,\,k(-)} - \hat{\boldsymbol{x}}_{k(-)}][\boldsymbol{\chi}_{j,\,k(-)} - \hat{\boldsymbol{x}}_{k(-)}]^T + \boldsymbol{Q}_k, \tag{18}$$

$$\boldsymbol{Z}_{j,k} = h(\boldsymbol{\chi}_{j,k(-)}, \boldsymbol{u}_k), \text{ for } j = 0, \ldots 2n, \tag{19}$$

$$\hat{\boldsymbol{z}}_{k(-)} = \sum_{j=0}^{2n} \gamma_j^{(m)} \boldsymbol{Z}_{j,\,k(-)}, \tag{20}$$

$$\boldsymbol{P}_{k(-)}^{zz} = \sum_{j=0}^{2n} \gamma_j^{(c)} [\boldsymbol{Z}_{j,\,k(-)} - \hat{\boldsymbol{z}}_{k(-)}][\boldsymbol{Z}_{j,\,k(-)} - \hat{\boldsymbol{z}}_{k(-)}]^T + \boldsymbol{R}_k, \tag{21}$$

$$\boldsymbol{P}_{k(-)}^{xz} = \sum_{j=0}^{2n} \gamma_j^{(c)} [\boldsymbol{\chi}_{j,\,k(-)} - \hat{\boldsymbol{x}}_{k(-)}][\boldsymbol{Z}_{j,\,k(-)} - \hat{\boldsymbol{z}}_{k(-)}]^T, \tag{22}$$

$$\boldsymbol{K}_k = \boldsymbol{P}_{k(-)}^{xz} (\boldsymbol{P}_{k(-)}^{zz})^{-1}, \tag{23}$$

$$\hat{\boldsymbol{x}}_{k(+)} = \hat{\boldsymbol{x}}_{k(-)} + \boldsymbol{K}_k \left[\boldsymbol{z}_k - \hat{\boldsymbol{z}}_{k(-)}\right], \tag{24}$$

$$\boldsymbol{P}_{k(+)}^{xx} = \boldsymbol{P}_{k(-)}^{xx} - \boldsymbol{K}_k \boldsymbol{P}_{k(-)}^{zz} \boldsymbol{K}_k^T. \tag{25}$$

4. SUB-OPTIMAL SLIDING MODE CONTROL

The availability of an estimated EWS allows to design a controller that tracks a desired tip speed ratio (TSR) λ. For instance, maximum energy capture is obtained when

$$C_{\mathrm{P}}(\lambda^{\mathrm{opt}}, \theta^{\mathrm{opt}}) = C_{\mathrm{P}}^{\max}, \tag{26}$$

where λ^{opt} and θ^{opt} are the TSR and collective blade-pitch angles that maximize C_{P}. For this purpose, θ must track θ^{opt}, and the rotor speed ω_r should track

$$\omega_{\mathrm{r}}^{\mathrm{opt}} = \frac{\lambda^{\mathrm{opt}} \hat{v}_{\mathrm{w}}}{R}, \tag{27}$$

which indeed depends on the estimated EWS $\hat{v}_{\mathrm{w}}$. A control law for the generator torque T_{e} to track $\omega_{\mathrm{r}}^{\mathrm{opt}}$ via a quasi-continuous first-order SMC [13] is given as

$$T_{\mathrm{e}} = \frac{T_{\mathrm{a}}(\hat{v}_{\mathrm{w}}, \omega_{\mathrm{m}}, \theta^{\mathrm{opt}}) - J_{\mathrm{T}} \dot{\omega}_{\mathrm{r}}^{\mathrm{opt}} - a_1 s_1 - \alpha_1 sign(s_1)}{\eta_{\mathrm{g}}}, \tag{28}$$

which forces $s_1 = \omega_{\mathrm{r}}^{\mathrm{opt}} - \omega_{\mathrm{m}}$ to zero, with a_1 and α_1 being positive control parameters. Furthermore, the corresponding thrust force coefficient $C_{\mathrm{T}}(\lambda^{\mathrm{opt}}, \theta^{\mathrm{opt}})$ can be derived at these optimal operation conditions. Accordingly, decreasing the tip speed ratio from its optimum value causes a significant reduction in thrust compared to its reduction in power as seen in Fig.1. The curves were computed with the identified steady-state turbine model. For example, with a tip-speed ratio of approximately 6, the reduction in power is about 10%, while the reduction in thrust is 20%. Therefore, from (27), we can freely decide a sub-optimal operation condition $\lambda^{\text{sub-opt}}$ that satisfies a desired reduction of aerodynamic load and power, appropriately.

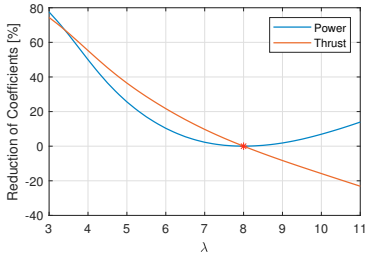

Fig. 1. Power and thrust coefficients analysis of the DTU 10 MW RWT: corresponding power and thrust reductions (the marked point represents the optimal operation, $\lambda^{\mathrm{opt}} = 8$)

Remark 1. Depending on the energy prices and the savings on lifetime extension due to load reduction, an optimization problem can be formulated to find the appropriate sub-optimal conditions. Also, sub-optimal conditions could guarantee modified safety levels due to damage or degradation. However, these are out of the scope of this work.

Remark 2. The stability analysis is herein omitted and provided in [13] for the controller. Still, if the wind estimator has a slow convergence, it can affect the closed-loop performance and lead to stall operation conditions [20]. In these conditions, un-modeled dynamics will be present in (2), which can lead to instability. The in-depth closed-loop performance and stability analysis are the aim of further work.

5. SIMULATIONS

In this section, we assess the performance of the UKF-based wind speed estimator via the high-fidelity Simulator for Wind Farm Applications (SOWFA) developed by the National Renewable Energy Laboratory (NREL) [3]. First, the estimators are tested under a refined mesh model, turbulent wind inflow, and high-waked scenario. Thus, in Section 5.1, a two-turbine wind farm composed of the DTU 10 MW reference wind turbine (RWT) with $5D$ distancing is used with the actuator line model advanced (ALMAdvanced) solver. Then, in Section 5.2, simulations with FASTv8.16.00 [6], using BeamDyn, were conducted to validate the use of the estimators, despite the non-modeled structural dynamics. The single NREL 5 MW RWT was used in turbulent conditions. Finally, the last objective is to investigate the closed-loop system's performance with a controller. In Section 5.3, the optimal and the proposed sub-optimal SMC that uses the estimated EWS is tested in SOWFA. The sub-optimal SMC is presented herein as a solution for a required load reduction. The adopted parameters are included in Table 1.

5.1 Turbulent Simulations in SOWFA

Realistic simulations of a two-turbine wind farm were performed with a turbulent inflow field, approximately TI=5-6%, and mean inflow wind speed of 15 and 12 m/s at the hub height are performed using a "precursor" atmospheric large-eddy simulation (ABLSolver) with neutral atmospheric stability. A cubic cell length of 2.5 m near the rotors with a smearing factor of 5.0 m was used.

The proposed UKF-based estimator has presented better root-mean-squared errors of the estimated EWS compared with the other estimators over the entire simulation time - see Table 2. In addition, the root-mean-squared error between the measured and the estimated rotor speed, called innovation term or residual in the KF theory, is practically maintained by the UKF-based estimator compared to the EKF-based estimator. The result can also be visualized in Fig. 2. Even though high performance is obtained by the improved I&I technique, an important limitation has been observed. In order to expand the mathematical model, for instance, to include tower dynamics in the estimator, the conditions for the I&I estimator consistency [15] have to be further expanded, which is a non-trivial task to achieve.

Table 1. Estimator Parameters

Parameters	Attributed Values
$\sigma^2(w_p)$ [EKF; UKF]	1e-03 $[rad^2/s^2]$
$\sigma^2(w_v)$ [EKF; UKF]	0.1 $[m^2/s^2]$
$\sigma^2(v)$ [EKF; UKF]	0.1 $[rad^2/s^2]$
α [UKF]	1.22
β [UKF]	0.5
κ [UKF]	0
$\gamma_{I\&I}$ [I&I]	5
$\gamma_{I\&I}$ [Improved I&I]	40
$\beta_{I\&I}$ [Improved I&I]	10
Δt	0.2 (SOWFA) and 0.1 (FAST) $[s]$
Initial conditions	**Attributed Values**
$\hat{\omega}_r(0)$	1 $[rad/s]$
$\hat{v}_w(0)$	14 and 4 $[m/s]$
$\boldsymbol{P}_0^{xx}$	[1 0;0 1]

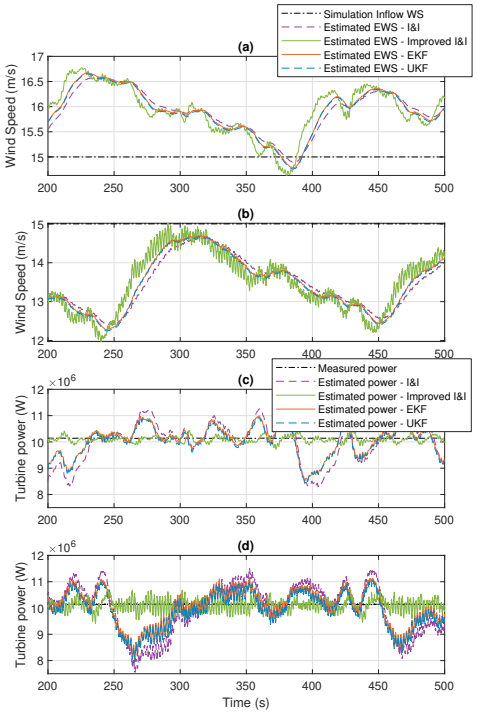

Fig. 2. (a) and (c) estimated EWS and derived power of the upstream; and (b) and (d) of the downstream DTU 10MW RWT at a mean inflow wind speed of 15 m/s with ALMAdvanced solver

Moreover, we observed that the theoretical variance of the estimated EWS, i.e $\boldsymbol{P}^{xx}_{k(+)}(2,2)$, from the UKF-based estimator is smaller than from the EKF-based estimator, depicted in Fig. 3. This is due to the nonlinear effects by the UT against the linearization procedure into the state covariance propagation and it elucidates the superior performance of the UKF.

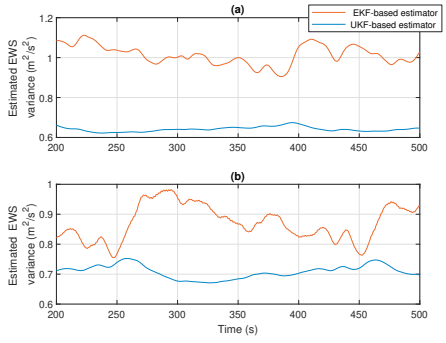

Fig. 3. Estimated EWS variance of (a) the upstream and (b) the downstream DTU 10MW RWT at mean inflow wind speed of 15 m/s with ALMAdvanced solver

Since the true EWS is unknown, we will instead compare the different filters by numerically evaluating the covariance of the estimation error with respect to the measured power signal P_{m}:

$$\bar{e}_{\mathrm{P},k} = \frac{1}{m}\sum_{t=k-m}^{k} e_{\mathrm{P},t}, \quad \text{where } e_{\mathrm{P},t} = P_{\mathrm{m}}(t) - \hat{P}(t); \tag{29}$$

Table 2. Signal Analysis of Turbulent Simulations

	RMS($\hat{v}_w$) [ms^{-1}]				RMS($\omega_m - \hat{\omega}_r$) [.10^{-4} rad/s]		
Simulations [200-500 s]	I&I	Imp I&I	EKF	UKF	Imp I&I	EKF	UKF
UpDTU10MW (15 m/s)	15.9217	15.9381	15.9281	15.9075	31	28	28
DownDTU10MW (15 m/s)	13.478	13.5145	13.4847	13.4539	46	43	42
UpDTU10MW (12 m/s)	12.4218	12.4215	12.4225	12.4039	12	19	19
DownDTU10MW (12 m/s)	8.4273	8.4274	8.4280	8.4058	24	29	29
(FAST)NREL5MW (15 m/s)	15.9968	16.0098	15.9864	15.9807	147	126	123
(FAST)NREL5MW (12 m/s)	12.2973	12.3273	12.3080	12.2982	113	95	92

$$\mathrm{cov_k}(e_P) \approx \frac{1}{m} \sum_{t=k-m}^{k} [e_{P,t} - \bar{e}_{P,t}]^2, \tag{30}$$

where $\hat{P}$ is the estimated power using the corresponding estimated EWS, and $m = 100$ s $/\,\Delta t$ is the length of the moving window used in the computation. The numerical result, depicted in Fig. 4, shows an improvement of the UKF over the EKF, even if it has been obtained by using a single simulation.

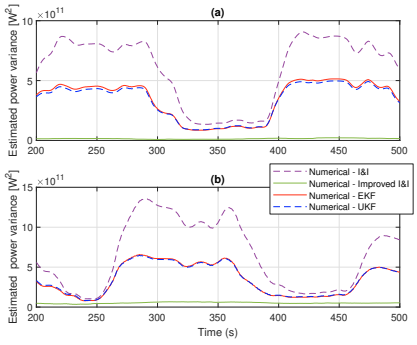

Fig. 4. Estimated power variance of (a) the upstream and (b) the downstream DTU 10MW RWT at mean inflow wind speed of 15 m/s with ALMAdvanced solver

Furthermore, the proposed UKF-based estimator has presented more robustness to initial conditions than the EKF-based estimator. This problem is also seen, for instance, in the spacecraft attitude estimation problem in [4].

5.2 *Turbulent Simulations in* FAST

In order to verify the effects of the tower dynamics, we use FASTv8.16.00 simulator (FAST) at a time step of 0.001 s where the estimators are implemented keeping the sampling time $\Delta t = 0.1$ s. The obtained results are also consistent at the inflow wind speed of 12 and 15 m/s and higher turbulence (approximately TI=11%) using the Kaimal turbulence model [7]. The estimators with the simplified model, i.e. Eq. (5) and Eq. (6), have still presented consistency on the estimated EWS even though more physics are coupled in the wind turbine dynamics, as seen in Fig. 5.

5.3 *Sliding mode control and sub-optimal operation*

The SOWFA simulation results of the two NREL 5MW RWT wind farm, at turbulent conditions (TI 5-6%) and control parameters: $a_1 = 4,326,000$ Nm/s and $\alpha_1 = 1,442$ Nm, is illustrated by Fig. 6. The upstream turbine, represented by the first-column plots, obtains the expected

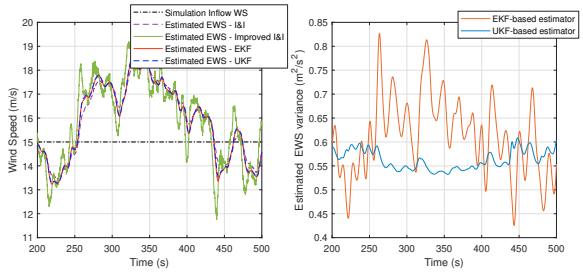

Fig. 5. Estimated EWS and varianve of the NREL 5MW RWT at mean wind speed of 15 m/s with FAST

result by reducing the power and thrust accordingly. However, in the downstream turbine, the performance deteriorates due to the un-modeled wake effects on the estimation and control. As a result, the optimal control of the downstream turbine using SMC is producing less power than the baseline controller, i.e. the classical ω_r^2-torque law, and the sub-optimal SMC reduces the loads but not significantly.

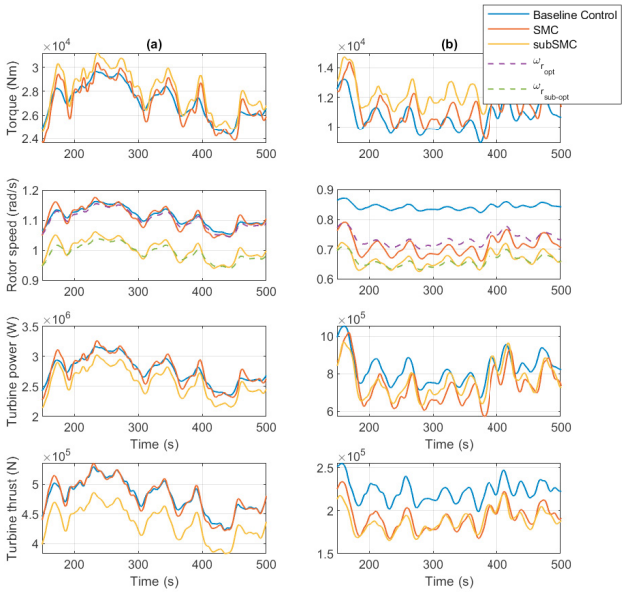

Fig. 6. SMC ($\lambda_{opt} = 7.55$) and subSMC ($\lambda_{sub-opt} = 6.795$) using the UKF-based EWS compared to the baseline controller at mean inflow wind speed of 9 m/s: (a) the upstream and (b) the downstream NREL 5MW RWT

6. CONCLUSIONS

The present paper has shown the advantages of estimating the effective wind speed via an unscented Kalman filtering technique. Firstly, the consistency of the proposed

estimator is maintained in high-waked scenarios and non-modeled structural dynamics. Secondly, the performance is improved in high wind speeds against the EKF due to the Unscented Transformation in the high nonlinear relation of the wind turbine system. Furthermore, compared with the I&I technique, the KF-defined residuals in the general formulation can be used in the development of fault detection algorithms. Also, the KF formulation can be easily extended to include more complex models, e.g. structural dynamics and even extra unknown inputs.

The knowledge of the wind speed, not required in the baseline controller, allows a real-time load reduction according to the current turbine operation. This might be beneficial in a long term or when it is required as a safety measurement. Yet, combining real-time estimation and control in the presence of non-modelled dynamics, due to the high-waked conditions, is shown to be an open challenge. In a closed loop with the SMC, satisfactory results were obtained for the upstream turbine as expected. However, at the downstream turbine, the closed-loop system presents a lower performance in terms of power production compared with the baseline controller.

Future work will investigate the adaptation of the noise statistics as in [19, 18] to increase the consistency of the state estimations under waked conditions and the tuning autonomy. Additionally, the presented methodology will be extended to more complex models, including for instance a flexible tower structure and sea wave dynamics.

ACKNOWLEDGEMENTS

The authors would like to acknowledge the WATER-EYE project. This project has received funding from the European Union Horizon 2020 research and innovation programme under the call H2020-LC-SC3-2019-RES-TwoStages.

REFERENCES

[1] Boersma, S. et al. (2017). A tutorial on control-oriented modeling and control of wind farms. In *American Control Conf.*, 1–18.

[2] Boersma, S. et al. (2019). A constrained wind farm controller providing secondary frequency regulation: An LES study. *Renewable Energy*, 134, 639–652.

[3] Churchfield, M.J. et al. (2012). A numerical study of the effects of atmospheric and wake turbulence on wind turbine dynamics. *J. of Turbulence*, 13, N14.

[4] Crassidis, J.L. and Markley, F.L. (2003). Unscented filtering for spacecraft attitude estimation. *J. of Guidance, Control, and Dynamics*, 26(4), 536–542.

[5] Griffith, D.T. et al. (2014). Structural health and prognostics management for the enhancement of offshore wind turbine operations and maintenance strategies. *Wind Energy*, 17(11), 1737–1751.

[6] Jonkman, J. and Jonkman, B. (2016). Nwtc information portal (fast v8.16.00). URL `https://www.nrel.gov/wind/nwtc/fastv8.html`. Accessed Fev. 20, 2021.

[7] Jonkman, J.B. and Kilcher, L. (2012). Turbsim user's guide: Version 1.06.00. URL `https://www.nrel.gov/wind/nwtc/turbsim.html`. Accessed Fev. 20, 2021.

[8] Julier, S.J., Uhlmann, J.K., and Durrant-Whyte, H.F. (1995). A new approach for filtering nonlinear systems. In *American Control Conf.*, 1628–1632 vol.3.

[9] Kalman, R.E. (1960). A new approach to linear filtering and prediction problems. *J. Basic Eng.*, 82(1), 35–45.

[10] Knudsen, T., Bak, T., and Soltani, M. (2011). Prediction models for wind speed at turbine locations in a wind farm. *Wind Energy*, 14(7), 877–894.

[11] Lio, W.H., Li, A., and Meng, F. (2021). Real-time rotor effective wind speed estimation using gaussian process regression and kalman filtering. *Renewable Energy*, 169, 670–686.

[12] Liu, Y. et al. (2022). The immersion and invariance wind speed estimator revisited and new results. *IEEE Control Systems Letters*, 6, 361–366.

[13] Mérida, J., Aguilar, L.T., and Dávila, J. (2014). Analysis and synthesis of sliding mode control for large scale variable speed wind turbine for power optimization. *Renewable Energy*, 71, 715–728.

[14] Menegaz, H.M.T. et al. (2015). A systematization of the unscented kalman filter theory. *IEEE Trans. on Automatic Control*, 60(10), 2583–2598.

[15] Ortega, R., Mancilla-David, F., and Jaramillo, F. (2011). A globally convergent wind speed estimator for windmill systems. In *Conf. on Decision and Control and European Control Conf.*, 6079–6084.

[16] Østergaard, K.Z., Brath, P., and Stoustrup, J. (2007). Estimation of effective wind speed. *J. of Physics: Conference Series*, 75, 012082.

[17] Pao, L.Y. and Johnson, K.E. (2011). Control of wind turbines. *IEEE Control Systems Mag.*, 31(2), 44–62.

[18] Ritter, B. et al. (2019). Adaptive master-slave cubature Kalman filters subject to state inequality constraints for wind turbine state estimation. In *American Control Conf.*, 3482–3487.

[19] Silva, J.G., Aquino Limaverde Filho, J.O.D., and Feitosa Fortaleza, E.L. (2018). Adaptive extended kalman filter using exponential moving average. *IFAC-PapersOnLine*, 51(25), 208 – 211.

[20] Silva, J.G., Ferrari, R., and van Wingerden, J.W. (2022). Convex model predictive control for down-regulation strategies in wind turbines. In *Conf. on Decision and Control*, 3110–3115. IEEE.

[21] Silva, J.G., Ferrari, R., and van Wingerden, J.W. (2023). Wind farm control for wake-loss compensation, thrust balancing and load-limiting of turbines. *Renewable Energy*, 203, 421–433.

[22] Simley, E. and Pao, L.Y. (2016). Evaluation of a wind speed estimator for effective hub-height and shear components. *Wind Energy*, 19(1), 167–184.

[23] Sloth, C., Esbensen, T., and Stoustrup, J. (2010). Active and passive fault-tolerant lpv control of wind turbines. In *American Control Conf.*, 4640–4646.

[24] Soltani, M.N. et al. (2013). Estimation of rotor effective wind speed: A comparison. *IEEE Trans. on Control Systems Technology*, 21(4), 1155–1167.

[25] Wan, E.A. and Van Der Merwe, R. (2000). The unscented kalman filter for nonlinear estimation. In *Procs. of the Adaptive Systems for Signal Proccessing, Communications, and Control Symposium*, 153–158.